N. Jb. Geol. Paläont. Abh. 286/1 (2017), 75–95
Stuttgart, October 2017

Article

Geology, geochemistry and microthermometry of Mn-bearing hydrothermal veins near Birjand, east Iran

Behnaz Barghi, Ali Asghar Calagari, Mohammad Hossein Zarrinkoub and Vartan Simmonds

With 15 figures and 2 tables

Abstract: Mn-bearing veins in three prospect (Beshgaz, Sehchangi, and Basiran) near Birjand, east Iran are hosted by Paleogene andesitic lavas (Eocene) and dacitic-rhyodacitic tuffs (Eocene-Oligocene). The major opaque minerals in the veins are pyrolusite, cryptomelane, psilomelane, hollandite, hematite, goethite, and limonite mainly having colloidal and open-space filling textures. The major non-opaque gangue minerals are gypsum, halite, barite, calcite, and silica. Alteration halos (mainly argillic and silicic) developed in the wall rocks of the veins and veinlets. X-ray diffraction and geochemical data indicate that the primary manganese minerals were deposited in as amorphous oxy-hydroxides. Recrystallization to psilomelane and hollandite, and then to pyrolusite occurred at the expense of the primary amorphous minerals. The average Mn/Fe ratios of the ores in Beshgaz, Sehchangi, and Basiran are 26.31, 48.55, and 1.81, respectively, and indicate that the Mn ores formed from hydrothermal fluids. Fluid inclusions study demonstrates that the ore-forming solutions had salinities within the range 0.5-5.5 wt% NaCl eq., and homogenization temperatures in the range 120-220 °C. The pressure is estimated to be about 50 bars, corresponding to a depth of ore vein formation of ~150 meters.

Key words: Mn veins; Pyrolusite; Psilomelane; hollandite; Birjand; Beshgaz; Sehchangi; Basiran; Fluid inclusion; Hydrothermal.

Introduction

Numerous manganese deposits have been found in different parts of Iran, dating from the Late Proterozoic to Pliocene (Forster 1978; Laznicka 1992; Roy 2012; Samani 1988). The major manganese deposits of Iran are Tertiary in age and can be classified into three broad genetic types: sedimentary, volcano-sedimentary, and hydrothermal. The Mn mineralization mainly occurs in Eocene volcanic rocks, particularly andesitic-dacitic lavas, but is also reported from post-Eocene granitic intrusions (Forster 1978). Manganiferous iron ore formation in central Iran is thought to be associated with the pan-African metallogenic phase, during formation of the Posht Badam volcano-sedimentary deposits in what was probably a rift setting (Amidi et al. 1984; Foerster & Jafarzadeh 1994; Moore & Modabberi 2003). However, subduction-related Mn deposits, such as those at Venarch, Robat Karim, Chah basheh and Bozni (major Mn deposits), are considered to be the most important ones in Iran (Ghorbani 2013).

Manganese mineralization in the study areas is spatially associated with Tertiary volcanic rocks that formed above a subduction zone in eastern Iran. Up to

www.schweizerbart.de
DOI: 10.1127/njgpa/2017/0687
0077-7749/2017/0687 $ 5.25

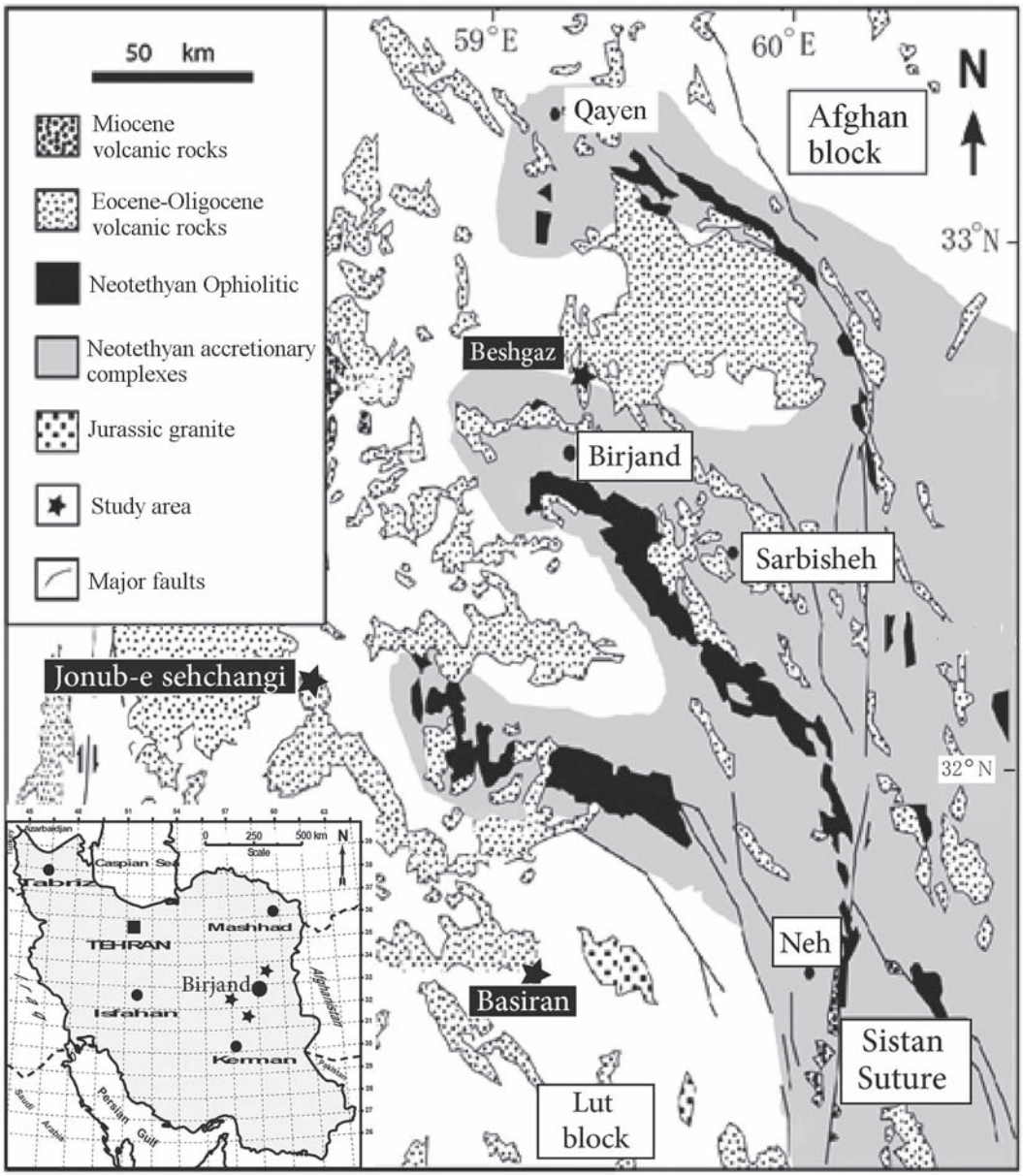

Fig. 1. Geology map showing the position of the three studied Mn prospect areas within the volcanic rocks of the Lut block in the eastern Iran.

date, no detailed studies on the manganese prospects at Beshgaz, Sehchangi, and Basiran have been carried out. The present study focusses on the petrology, mineralogy and geochemistry of these occurrences in combination with a microthermometry study on selected samples, in order to determine the source of the manganese and its relationship with the volcanic host rocks, the distribution of major, minor and trace elements between mineralized veins and host rock, and the physico-chemical conditions of the ore-forming fluids that formed the Mn-bearing veins. The results of these studies will be useful for manganese prospecting in the future.

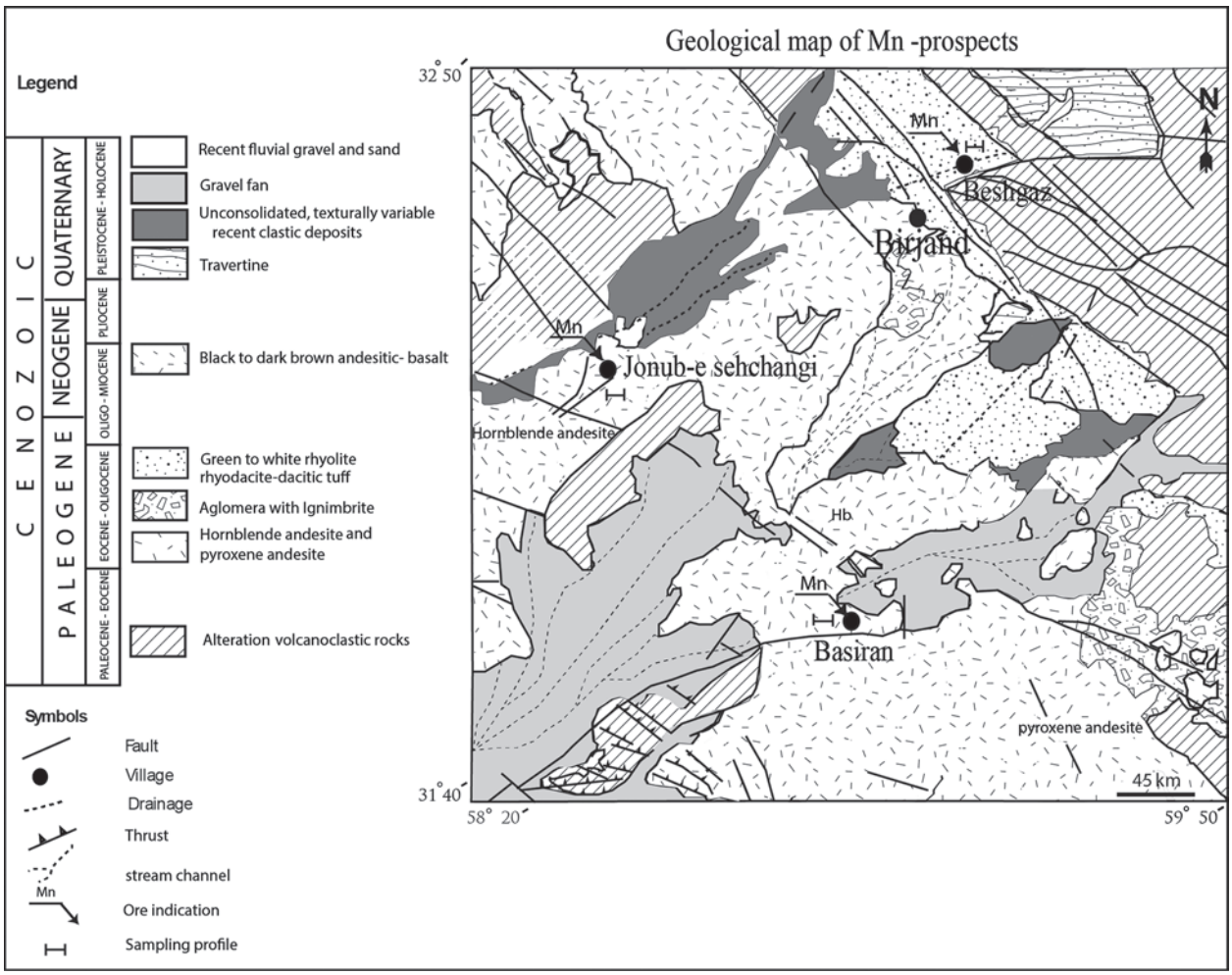

Fig. 2. Geology map of the studied areas (Beshgaz, Sehchangi, Basiran).

Methods

The field work for this study included the identification of the lithologic units (particularly of the host rocks), establishing the geometry of the ore bodies, mesoscopic examination of the ores, random and systematic collecting of samples (~90) across selected Mn-bearing veins, and finally the preparation of geologic maps of the prospected areas.

Subsequently, 76 thin-polished sections of selected host rock and ore samples were prepared for petrographic examination and, in addition, two doubly-polished wafers were prepared for fluid inclusion studies. Microthermometry analyses were carried out at the Iran Mineral Processing Research Center in Karaj using a Linkam-TH-600 stage.

Nineteen samples were selected for accurate identification of the constituent ore and gangue minerals by X-ray diffraction (XRD) analysis. XRD analyses were carried out at the Geology Department of the University of Birjand, using a model 1840 Phillips Diffractometer employing CuKα radiation and graphite chromators; operating condition were a 40 kV voltage, 30 mA current, 2° per minute scanning speed, and a 10-70° scan range. (Scan Axis Gonio, Start Position [°2θ] 4.0100, End Position [°2θ] 59.9900, Step Size [°2θ] 0.0200, Scan Step Time[s] 0.4000, Scan Type Continuous: Offset [°2θ] 0.0000, Divergence Slit Type Fixed: Divergence Slit Size [°] 1.0000, Specimen Length [mm] 10.00, Receiving Slit Size [mm] 0.1000, Measurement Temperature [°C] 0.00, Anode Material Cu, Generator Settings 40kV, 30mA, Diffractometer Type PW1840, Diffractometer Number 1, Goniometer Radius [mm] 173.00, Slit [mm] 91.00).

Furthermore, seventeen ore samples were selected for major, minor and trace element geochemistry at Acme labs, Canada, by induced-coupled plasma optical emission spectrometry and mass-spectrometry (ICP-ES and ICP-MS). The four acids digestion method was applied that dissolves most minerals: 0.25 g of sample material was heated in HNO3-HCIO4-HF mixture to fuming and then taken to dryness. The residue was dissolved in HCl and analyzed by ICP-ES or ICP-MS analysis. The results are listed in Table 1.

Geological setting

Regional geology

The three studied manganese prospect areas at Beshgaz, Sehchangi, and Basiran are situated in a structural zone known as the Lut Block. It constitutes the easternmost part of the central Iranian micro-continent and is bounded by the Nehbandan Fault to the east and the Nyband Fault to the west (Jung et al. 1983). The Lut block consists of Eocene volcanic rocks that formed during subduction of the Sistan Ocean between the Arabian and Turan plates and subsequent post-collisional tectonic activity (Berberian et al. 1999; Camp & Griffis 1982; Tirrul et al. 1983). Such Eocene volcanic rocks cover vast parts of eastern Iran (Richards et al. 2012) and are known to be highly prospective for Cu, Au, Pb, Zn, Fe (Lotfi 1982; Tarkian et al. 1983; Jung et al. 1983; Saadat et al. 2008, 2009; Walker et al. 2009; Arjmandzadeh et al. 2011, 2014). In contrast to the linear-shaped Urmea-Dokhtar volcanic belt, the volcanic rocks in the Lut Block are irregularly distributed between the Sistan suture zone in the east and the Nyband Fault in the west (Walker et al. 2009). The studied Mn prospects developed within these volcanic rocks (Fig. 1).

Geology of the studied areas

The Mn-bearing veins and veinlets are exposed in the Beshgaz, Sehchangi, and Basiran prospects located at, respectively, ~45 km, ~212 km, and 200 km northeast and southwest of Birjand. The important lithologic units in these areas, from the oldest to the youngest, are hornblende andesite (Eocene), pyroxene andesite (Eocene), green tuffs of rhyodacitic-dacitic composition (Eocene-Oligocene), lapilli tuffs made up of andesitic fragments (Eocene-Oligocene), andesitic basalt (Oligocene-Miocene), argillized tuffs (Pliocene), and Quaternary travertine (Fig. 2).

Petrography of the lithologic units

Dacitic and rhyo-dacitic tuffs: This unit hosts the Mn-bearing veins/veinlets in the Beshgaz area. The rocks are green is hand specimen and in thin section can be seen to consist mainly of plagioclase (50-60%) and quartz (~20%) set in a glassy matrix. Plagioclase varies in composition from albite to oligoclase and is partially altered to clay minerals.

Andesitic and andesi-basaltic lavas: These are dark gray in hand specimen and microscopically consists of plagioclase (65-70%), clinopyroxene (15-20%), hornblende (3-6%), and olivine (2-4%), showing porphyritic and fluvial textures. Plagioclase varies in composition from oligoclase to andesine and was partially altered to carbonate and clay minerals. Hornblende phenocrysts have opaque rims due to oxidation of the iron.

Hornblende and pyroxene andesite porphyry: The Mn-bearing veins/veinlets are hosted by hornblende andesite porphyry unit at Sehchangi, and by pyroxene andesite porphyry at Basiran. In hand specimen, these rocks are pink and exhibit conspicuous porphyritic textures. Under the microscope, the samples from Sehchangi consists of plagioclase (65-79%) and ferromagnesian minerals (~30%, principally hornblende), while the chief ferromagnesian mineral at Basiran is clinopyroxene. Plagioclase is mainly andesine-labradorite and partially altered to clay and carbonate minerals and accessory amounts of epidote. Locally, aggregates of plagioclase phenocrysts form a glomeroporphyritic texture. These samples also contain veinlets of carbonate minerals, silica (quartz), and zeolite (chabazite).

Mineralization

Mineralization in the prospect areas occurs as veins and veinlets, encrustations and open-space fillings in faulted and fractured zones. The major trend of the mineralized veins in all these three Mn prospects corresponds with the trend of right lateral strike slip faults, such as the Nehbandan strike slip fault and splays of the Nehbandan Fault.

At Beshgaz, the mineralized zones developed as parallel to sub-parallel veins trending NW-SE, parallel to the NW-SE trend of the major fault (Fig. 3a, b, c). The veins/veinlets have widths varying from 1 cm to 1.5 m and have lengths up to 7 meters. The manganese reserve (with an average grade of 25%) is estimated to be ~10000 metric tons (Fig. 3 d). Mineralization is principally observed as open-space fillings within the volcanic breccias (tuffs) (Fig. 3e). In the argillic zones, the Mn-bearing veins/veinlets vary in width from 1 cm to 20 cm (Fig. 3f) and from 1 mm up to 40 cm within the silicic zones (Fig. 3g). The opaque minerals within these veins/veinlets have mainly colloform textures, and the surfaces of jasper are covered by a green coating of fibroferrite [$Fe(OH)(SO_4)(H_2O)_5$] (Fig. 3h, k, l).

At Sehchangi, the veins developed within hornblende andesite porphyry and have widths up to ~1.5

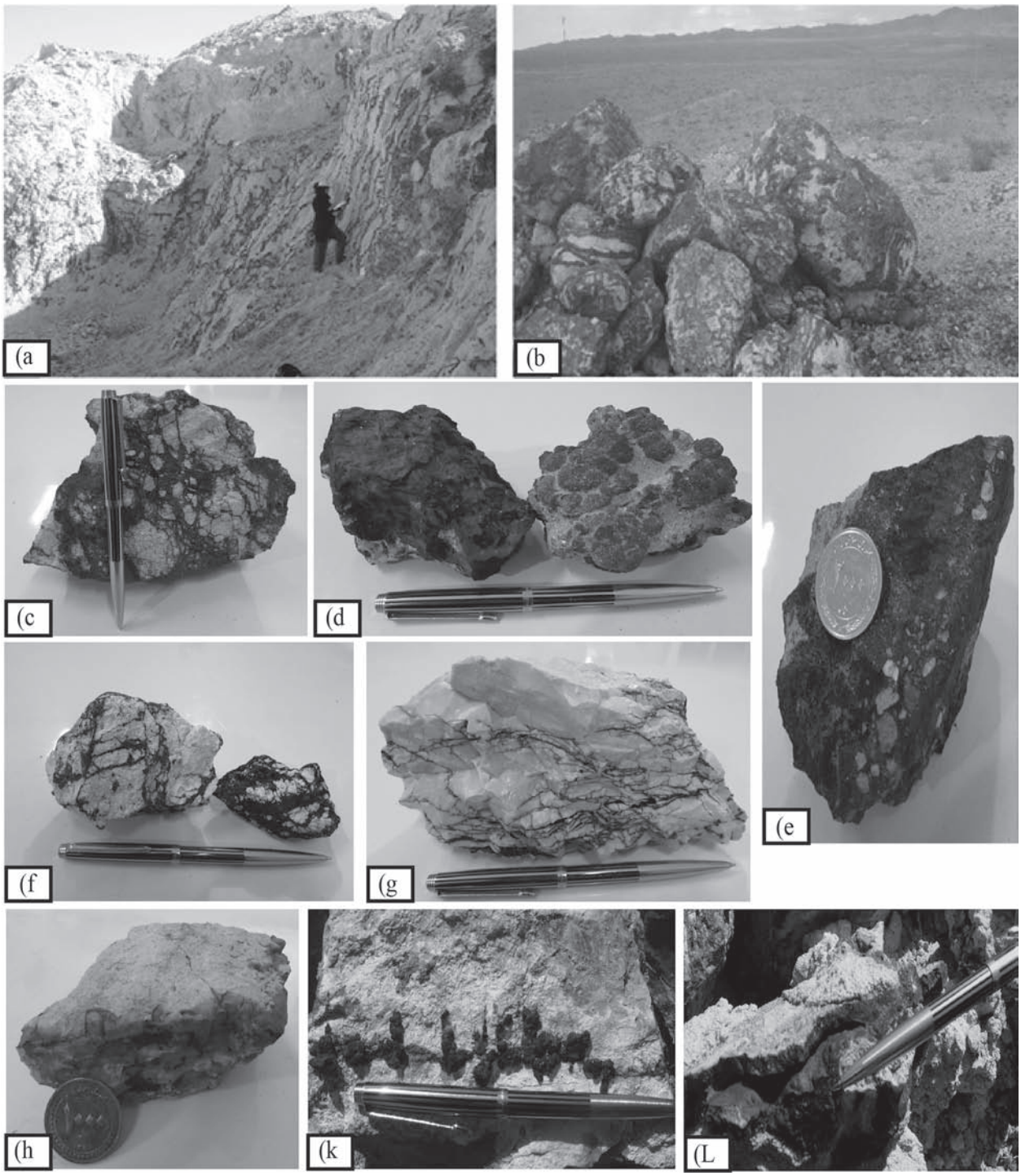

Fig. 3. (a) Parallel to sub-parallel veins within the pyroclastic unit (tuffs) at Beshgaz prospect. (b, c) Banded structure at Beshgaz prospect. (d) Mn minerals with botryoidal texture at Beshgaz prospect. (e) Open-space-filling within volcanic breccias at Beshgaz prospect. (f) Mn mineralization as veins within argillic zone at Beshgaz prospect. (g) Mn-bearing veins within cryptocrystalline silicic zone at Beshgaz prospect. (h) Mn-bearing veins within jasper at Beshgaz prospect. (k) Mn ore showing botryoidal texture within jasper at Beshgaz prospect. (l) Mn mineralization occurring as open-space filling within jasper at Beshgaz prospect.

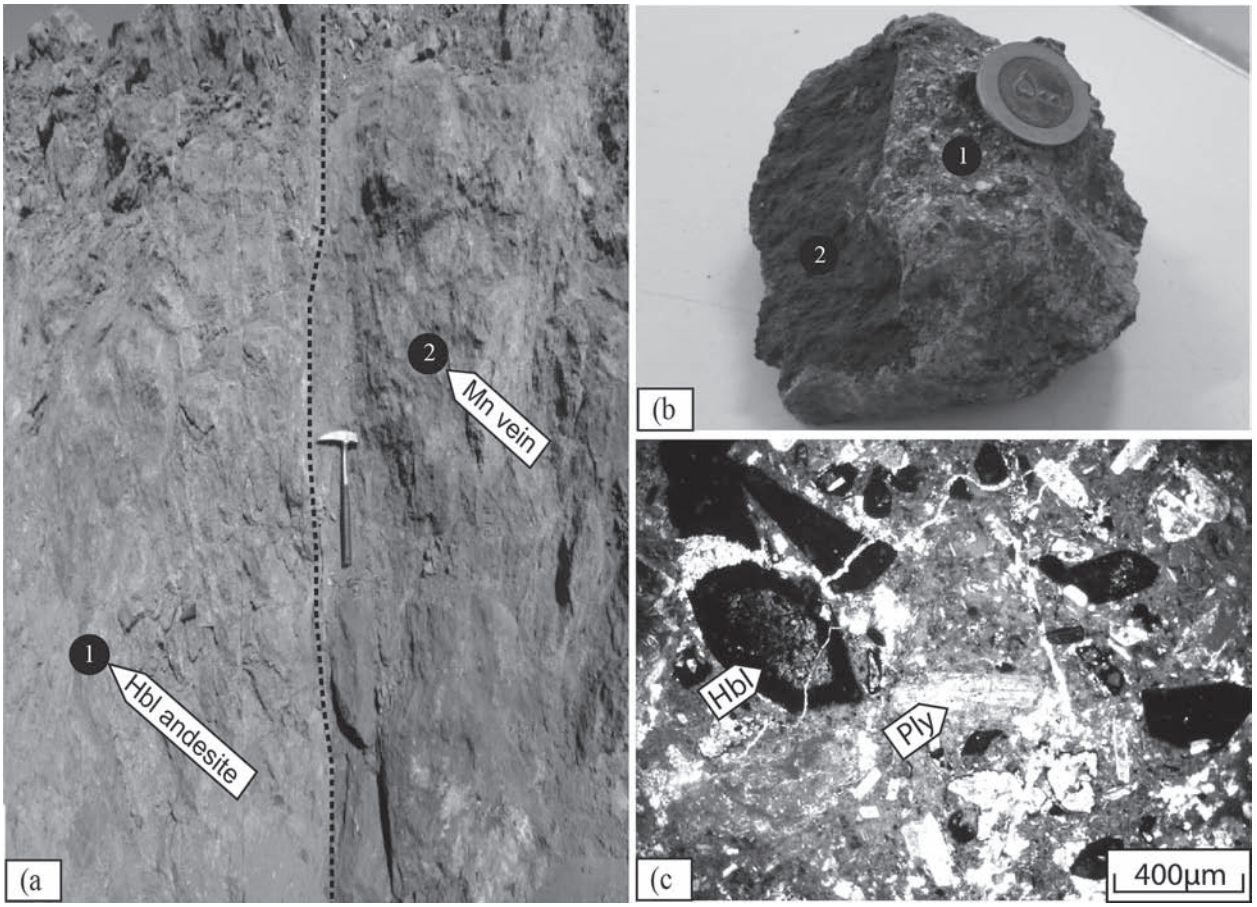

Fig. 4. (a, b) Mn-bearing veins hosted by hornblende andesite porphyry at Sehchangi prospect. (c) Photomicrograph of hornblende andesite porphyry showing phenocrysts of plagioclase and hornblende set in microlitic matrix at Sehchangi prospect.

m and lengths up to 3.5 m, trending E-W (Fig. 4a, b, c). The manganese reserve (with an average grade of 28%) was estimated to be ~100000 metric tons.

At Basiran, Mn mineralization also occurred as veins/veinlets and open-space fillings (Fig. 5a, b, c), and the Mn minerals are accompanied by Fe-oxides and -hydroxides (Fig. 5d) and galena (Fig. 5e). The individual veins have widths varying from 0.5 m to 3 m and extend up to 110 meters, trending N-S. The manganese reserve (with an average grade of 26%) is estimated to be ~11000 metric tons.

Alteration zones

The alteration zones in the prospect areas developed along the Nehbandan and Nayband faults defining the boundaries of the Lut Block. Argillic and silicic alteration is observed around the Mn-bearing veins at Beshgaz. Here, the argillic alteration zone varies in color from white to yellow, contains chiefly montmorillonite, and covers about 45 km^2 (Fig. 6a). The silicic alteration varies in color from white to red and brown, and contains amorphous silica (Fig. 6b). At Sehchangi and Basiran argillic alterations occur around the Mn-bearing veins and veinlets (Fig. 6c, d).

Ore petrography

Petrographic studies and XRD analyses show the ores at Beshgaz to consist of, in order of decreasing abundance, pyrolusite, psilomelane, and cryptomelane forming colloidal and open-space filling textures (Fig. 7a to

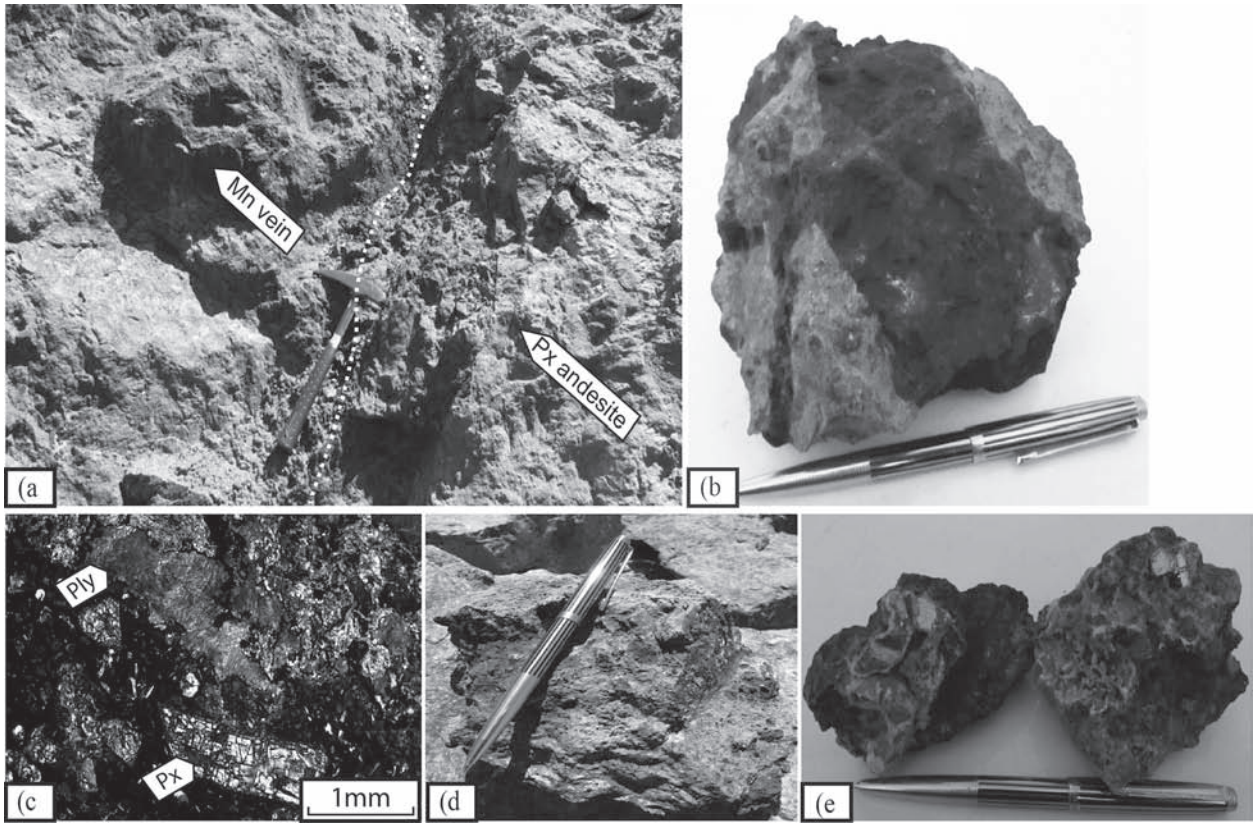

Fig. 5. (a, b) Mn-bearing veins hosted by pyroxene andesite porphyry at Basiran prospect. (c) Photomicrograph of pyroxene andesite porphyry showing plagioclase phenocrysts (plane polarized light, ppl) at Basiran prospect. (d) Pyrolusite accompanied by goethite and limonite at Basiran prospect. (e) Galena in the form of open-space filling along with pyrolusite at Basiran prospect.

d) Bentonite and silica are the major gangue minerals. The opaque minerals at Sehchangi are pyrolusite, psilomelane, cryptomelane, hollandite, hematite, goethite, and chalcopyrite displaying colloidal and open-space filling textures (Fig. 7e and f). Barite, halite, and gypsum are the major gangue minerals. The ores at Basiran include pyrolusite, psilomelane, hematite, goethite, limonite, and galena showing colloidal and open-space filling textures (Fig. 7g, h, k, l). Gypsum is the main non-opaque mineral at Basiran (Figs. 8, 9 and 10).

Geochemistry

The major, minor and trace element concentrations of the samples from the three prospects are listed in Table 1. Geochemical interpretation was based on Mn/Fe and Si/Al ratios, bivariate Ni/Zn versus (Ni+Co+Cu) and TiO_2 versus Al_2O_3 plots, and the Fe-Al-Mn ternary plot.

Major and minor elements: The correlations between these elements, the ratios of major to trace elements and the degree of enrichment of specific elements can be used to establish the source of the manganese (Shah et al. 1999; Polgari et al. 2012). Ratios of the major elements Mn, Fe, Ti, and Al are important indicators for the source and formation environment of Mn deposits (Karakus et al. 2010). Depending upon their solubilities, Mn and Fe can separate from each other at the time of deposition from hydrothermal fluids. Mn/Fe ratios of <1 indicate Mn deposition in lacustrine environments (Hein et al. 2000) and if the ratio is ~1, a hydrogenetic setting can be assumed (Nicholson 1992a; Rona 1987). If 0.1>Fe/Mn>10, the Mn deposit may

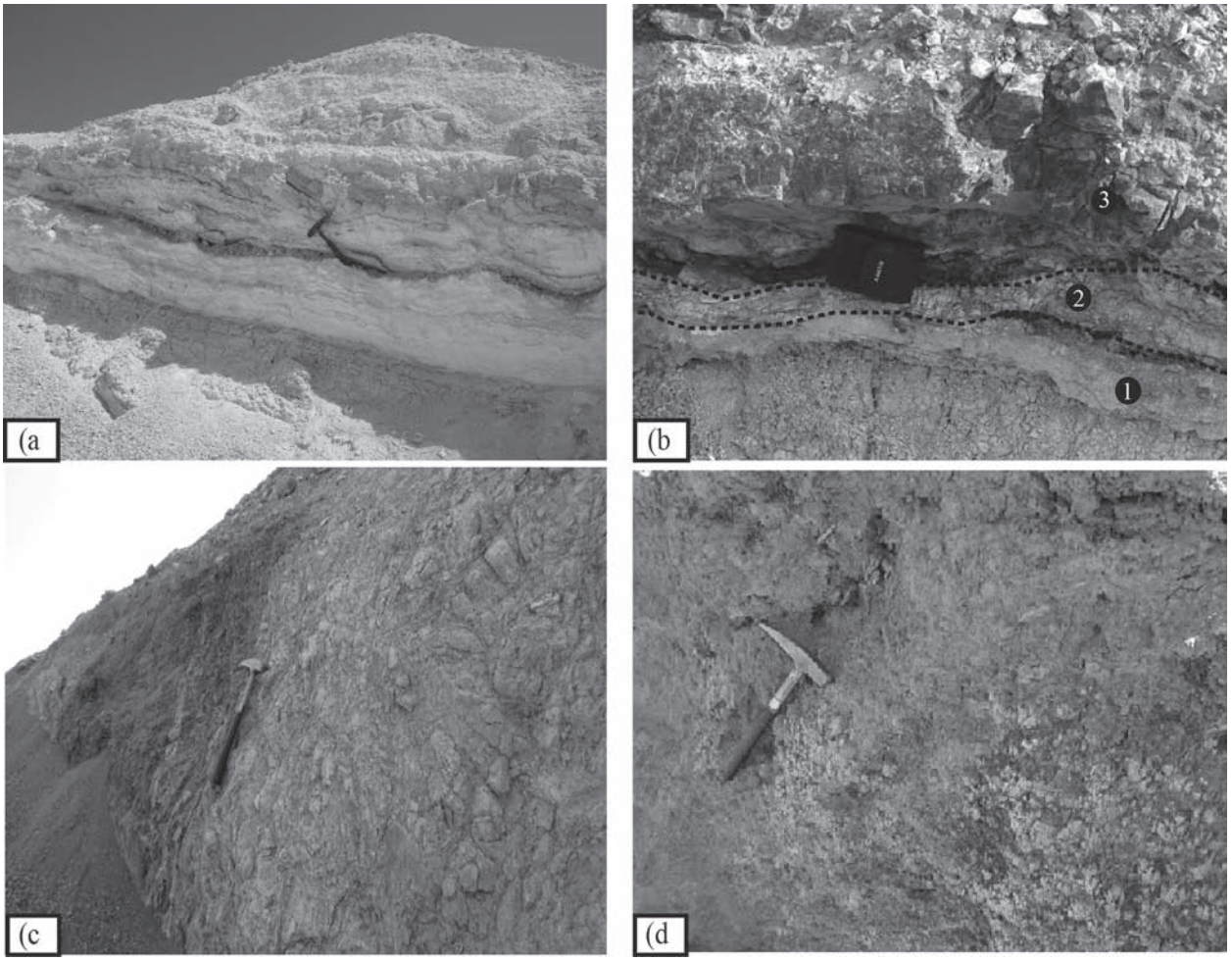

Fig. 6. (a) Argillic alteration in tuffs at Beshdaz prospect. (b) (1) Argillic, (2) White silicic alteration and (3) Red silicic alteration around Mn-bearing veins at Beshdaz prospect. (c) Argillic alteration in andesite at Sehchangi. (c) Argillic alteration in andesite at Basiran.

have a hydrothermal origin (Nicholson 1992b). Mn/Fe ratio means for the analyzed ore samples are 26.31 at Beshgaz, 48.55 at Sehchangi, and 1.81 at Basiran. Such ratios indicate a hydrothermal origin for the Beshgaz, Sehchangi and Basiran Mn prospects. Furthermore, Mn/Fe ratios >10 (as at Beshgaz and Sehchangi) indicate enrichment of Mn and its almost complete separation from Fe by hydrothermal processes.

The Si/Al ratio is another parameter that can be used to distinguish between hydrothermal, hydrogenous, and terrigenous Mn deposits, and can be used to identify the source of the Mn supplied to the depositional environment (Crerar et al. 1982; Bonatti 1975; Nicholson 1992b). Hydrothermal Mn deposits are commonly formed in connection with Fe-bearing siliceous gels, hence, Si/Al ratios are relatively high. In contrast, in terrigenous Mn deposits Al concentrations are greater than Si concentrations, which is due to the destruction of feldspars during erosion and transportation to the site of deposition (Roy 1992). Holtstam & Mansfeld (2001) suggest that Si/Al ratios of hydrothermal Mn deposits containing clay minerals may drastically decrease, and the Si/Al ratios mean for the analyzed ore samples 12.98 at Beshgaz, 3.14 at Sehchangi, and 7.3 at Basiran. Si/Al ratios of the studied Mn ores plot in the hydrothermal deposit field (Fig. 11a).

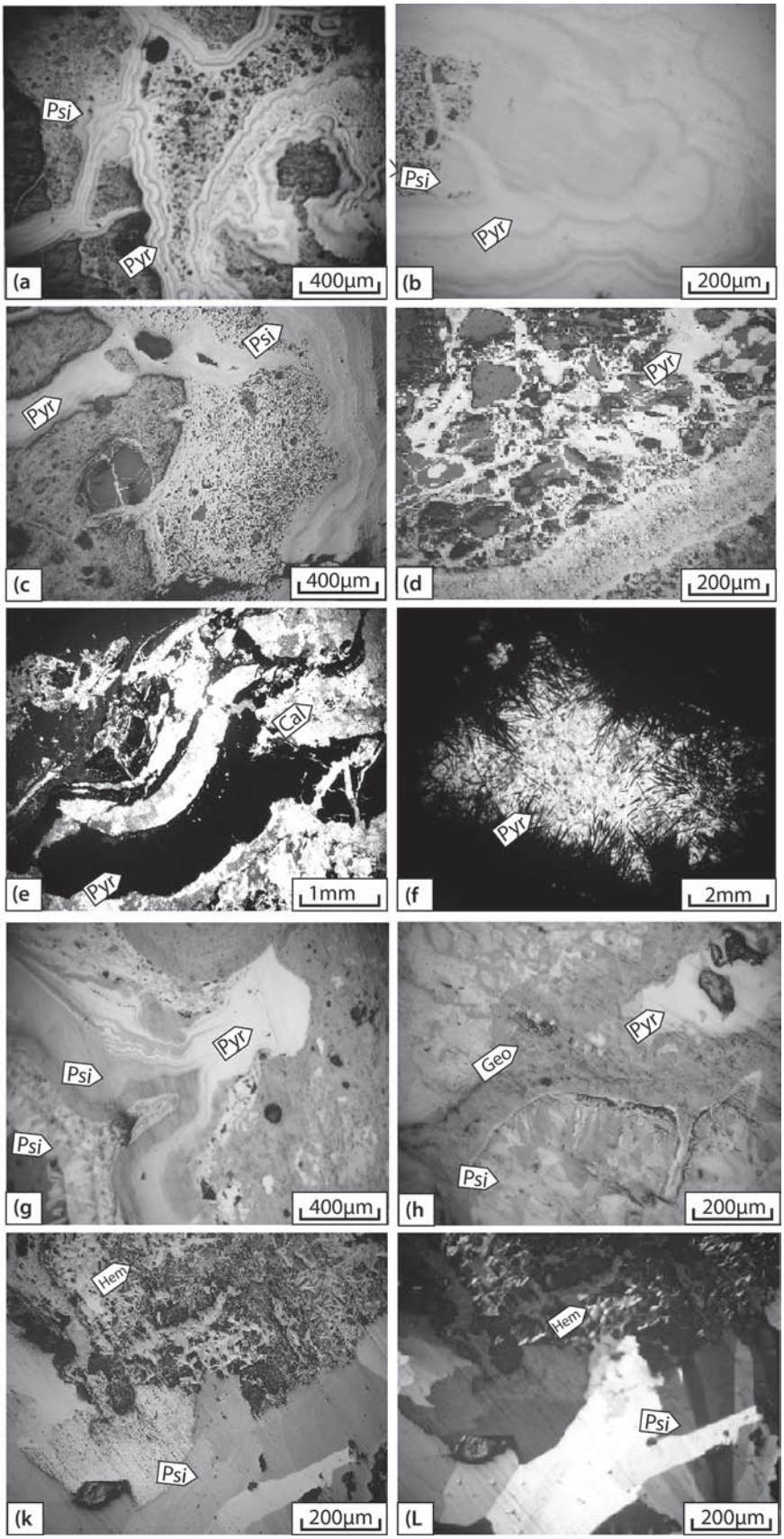

Fig. 7. Photomicrographs of Mn ores in the studied areas. (a, b) Colloidal texture (ppl) in the Beshgaz ore. (c, d) Open-space filling texture (ppl) in the Beshgaz ore. (e) colloidaltexture (cross polarized light, xpl) in the Sehchangi ore. (f) Open-space filling texture (xpl) in the Sehchani ore. (g) Colloidal texture (ppl) in the Basiran ore. (k) Acicular hematite beside psilomelane (ppl) in the Basiran ore. (i) Acicular hematite beside psilomelane (xpl) in the Basiran ore.

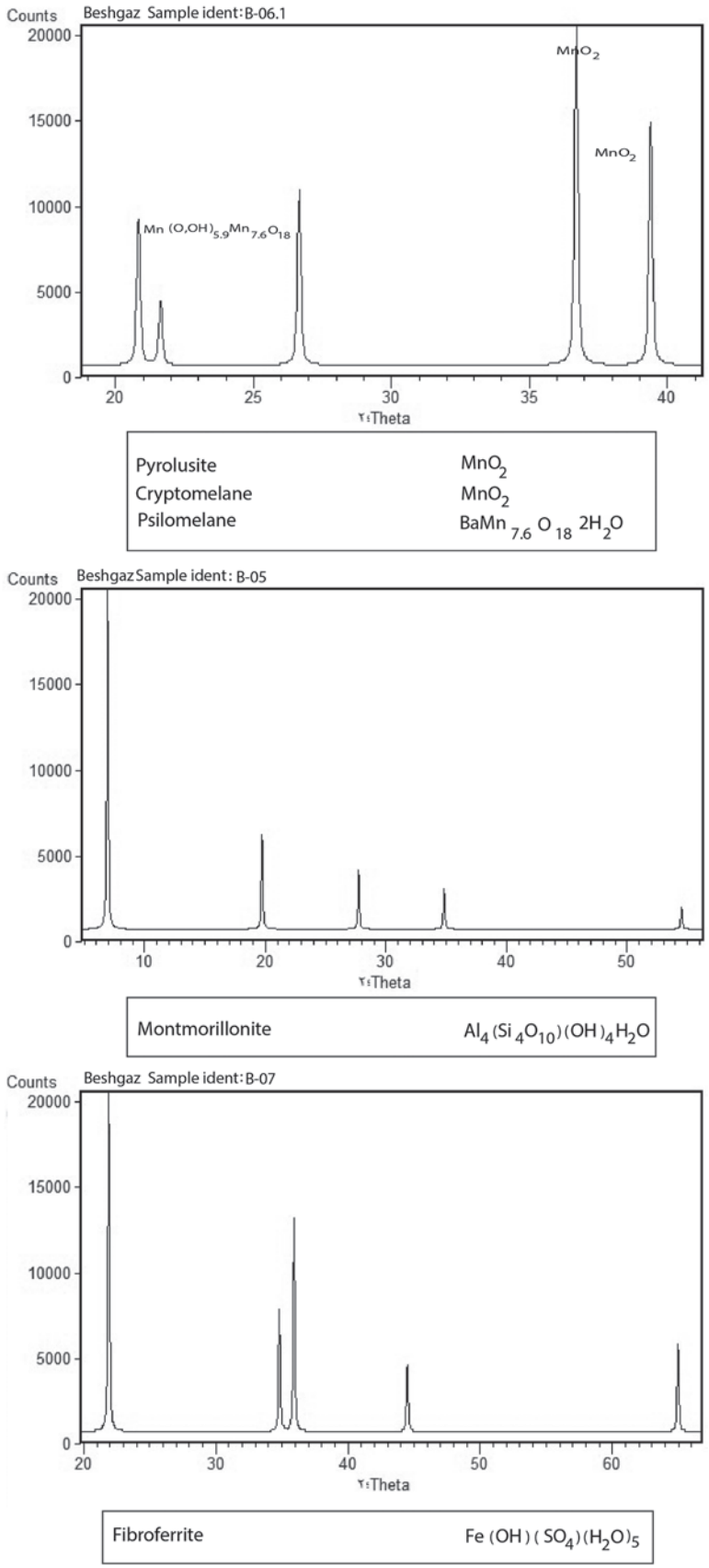

Fig. 8. XRD spectrum for an ore sample from the Beshgaz area. (samples B-06.1, B-05 & B-07, see Table 1).

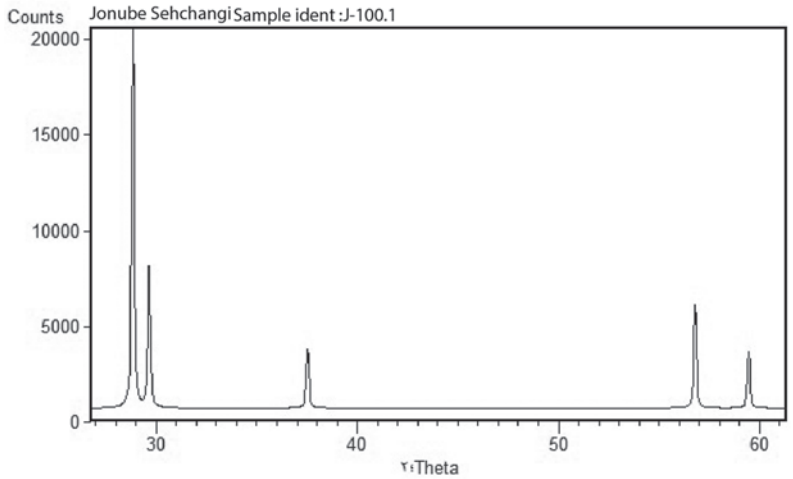

Pyrolusite	MnO_2
Cryptomelane	MnO_2
Psilomelane	$Ba\,Mn_{8.9}\,O_{18}\,2H_2O$
Hollandite	$Mn_{6.95}\,Fe_{0.64}\,Al_{1.26}Si$

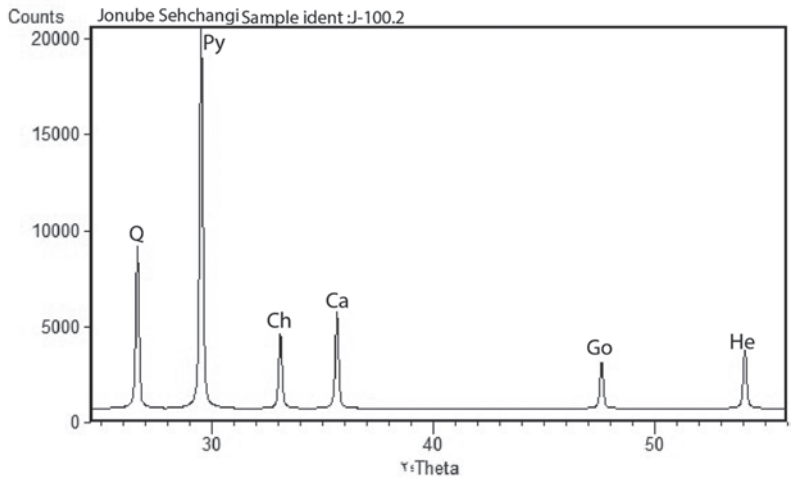

Pyrolusite	MnO_2
Hematite	Fe_2O_3
Goethite	$FeO(OH)$
Quartz	SiO_2
Calcite	$CaCO_3$
Chabasite	$(Ca,Na)_2Al_2Si_4O_{12}\cdot 6H_2O$

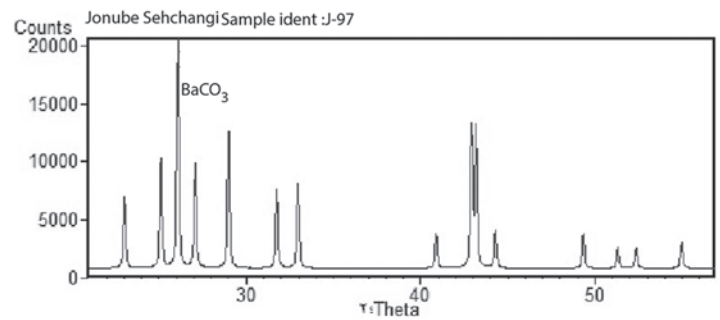

Barite	$BaCO_3$

Fig. 9. XRD spectrum for an ore sample from the Jonub–e Sehchangi area. (samples J-100.1, J-100.2 & J-97, see Table 1).

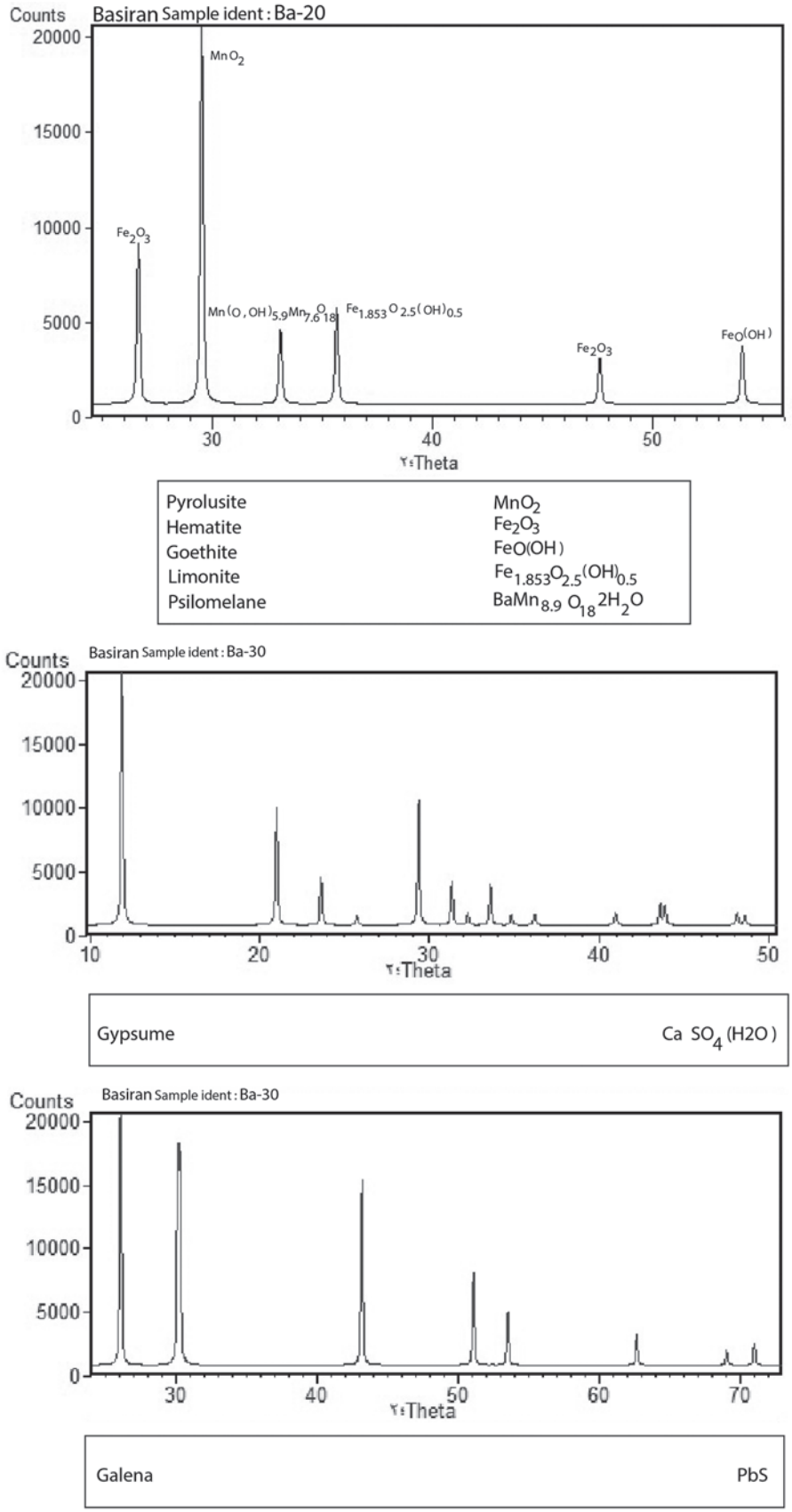

Fig. 10. XRD spectrum for an ore sample from the Basiran area. (samples Ba-20 & Ba-30, see Table 1).

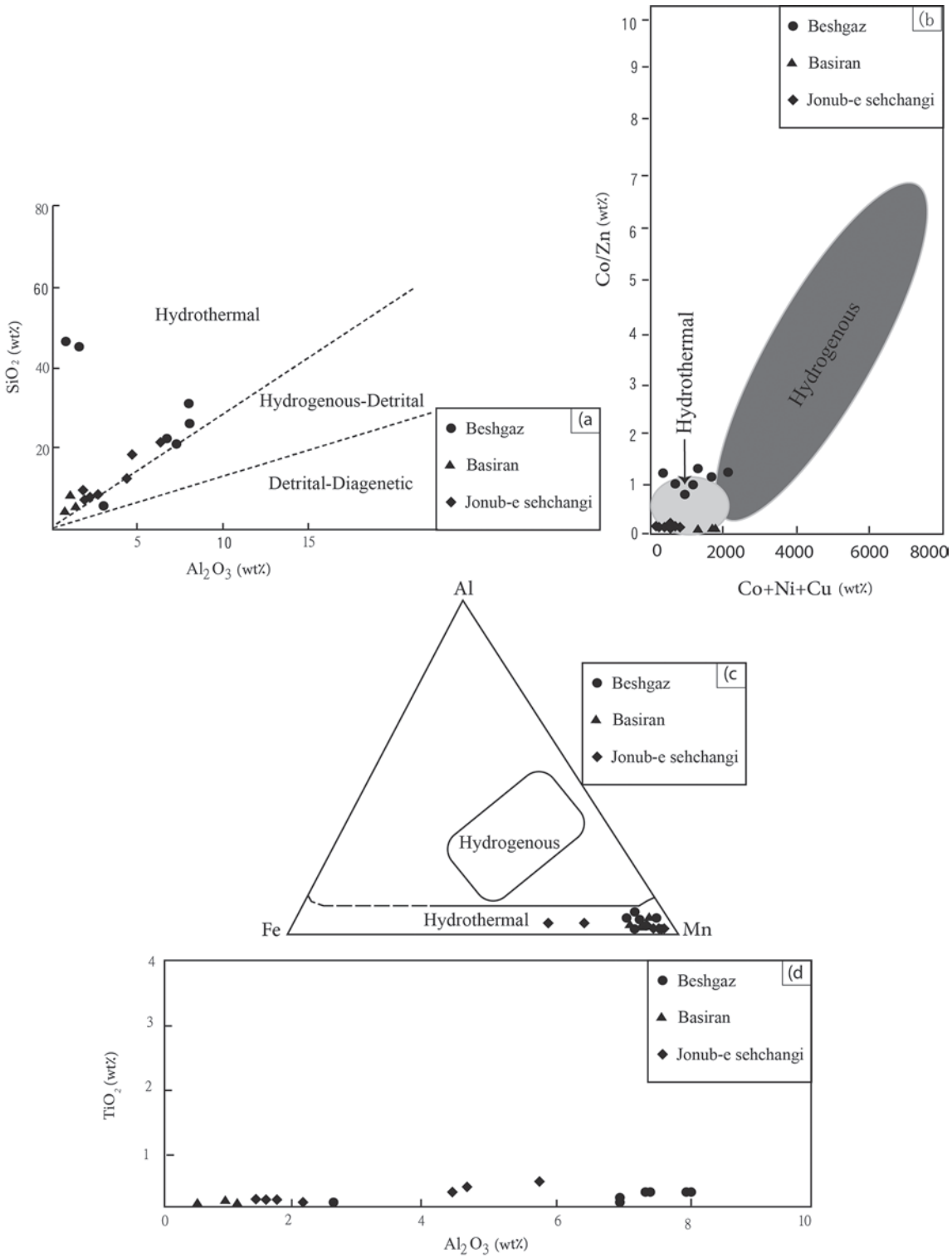

Fig. 11. (a) Bivariate SiO_2 versus Al_2O_3 plot (Choi & Hariya 1992) showing that Mn ores in the study areas lie in the hydrothermal field. (b) Bivariate plot of Co/Zn versus (Co+Ni+Cu) exhibiting that the studied Mn ores lie in the hydrothermal deposit field (Toth 1980). (c) Ternary plot of Fe-Al-Mn on which the data points of the studied Mn ores lie in the hydrothermal field (Adachi et al. 1986). (d) Bivariate plot of TiO_2 versus Al_2O_3 (Choi & Hariya 1992).

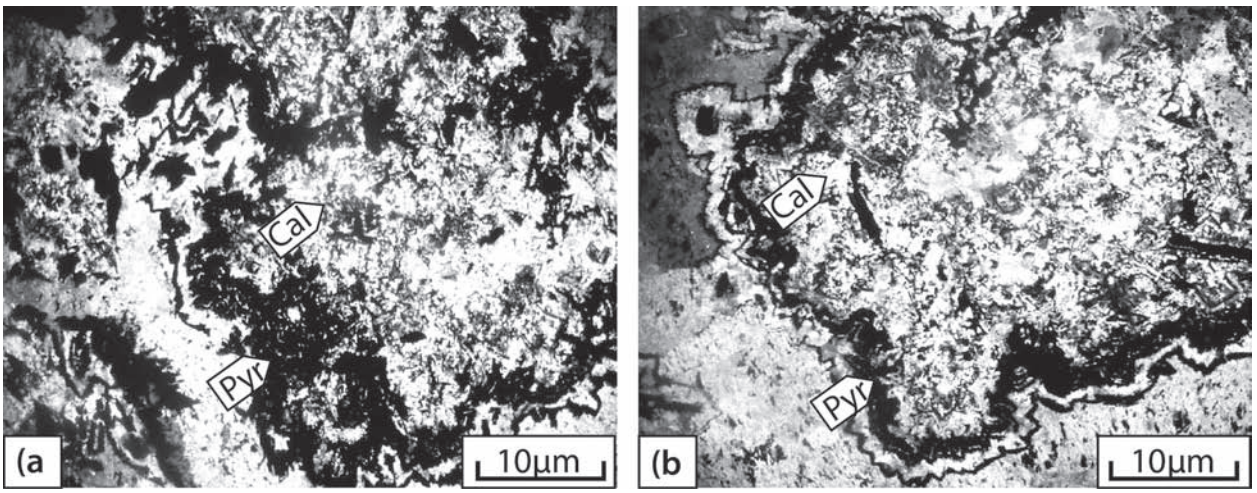

Fig. 12. Relationship between the Mn ore and gangue mineral calcite at the Basiran prospect.

The Ni/Zn versus (Ni+Co+Cu) plot was first used by Toth (1980) to distinguish hydrothermal Mn deposits from those of hydrogenous origin. Ni+Co+Cu totals of the ore samples are <200 ppm, and they plot in the hydrothermal deposit field (Fig. 11b).

The Fe-Al-Mn ternary plot presented by Adachi et al. (1986) illustrates that the Mn veins and veinlets in the studied prospects precipitated from hydrothermal fluids (Fig. 11 c). Moreover, the samples have low TiO_2 contents that correspond with low Al_2O_3 contents, indicating a hydrothermal origin for the Mn prospects (Fig. 11d).

Microthermometry

Fluid inclusion studies can provide good constraints for the physico-chemical conditions (temperature, pressure, and salinity) of ore formation and evolution of the ore-forming hydrothermal fluids (Roedder 1976, 1979; Spooner 1981). For this reason, six doubly-polished sections were prepared for the study of fluid inclusions in calcite and quartz crystals associated with the Mn minerals. Of these, 2 sections from Beshgaz contained <4 µm sized inclusions in quartz crystals, and 2 sections from the Sehchangi contained <4 µm sized inclusions in calcite crystals; due to their small size, these were deemed unsuitable for microthermometric analysis. Only two sections from Basiran contained inclusions within the range 1-20 µm in calcite crystals (Fig. 12a, b), and these were used for microthermometry. Twenty-six fluid inclusions in calcite crystals were analyzed for homogenization temperature (T_H) and salinity, and the results are listed in Table 2. Petrographic examinations show that three inclusion generations are present: (1) primary, (2) pseudo-secondary, and (3) secondary.

Inclusion shapes vary from rounded, sub-rounded, stretched, ellipsoidal (Fig. 13a, b, c, d), elongate (Fig. 13b), to rhombic (Fig. 13c, e); the majority are liquid-rich 2-phase (gas and liquid) inclusions. The secondary and pseudo-secondary inclusions are very small (1-5 µm) and form trails of beads delineating micro-fracture surfaces within calcite crystals (Fig. 13e, f). Therefore, almost all of the analyzed inclusions were of primary and liquid-rich 2-phase type.

Microthermometry analyses were principally performed on relatively large (>5 µm) and liquid-rich 2-phase inclusions. These have a limited range in salinity (0.5-5.5 wt% NaCl eq.; Fig. 14a) and homogenized into the liquid state. Their homogenization temperatures (T_H) vary from 120 °C to 220 °C (Fig. 14b). The T_H versus salinity plot (Fig. 15a) demonstrates that the inclusions trapped under-saturated fluids within the temperature range 120-220 °C under a pressure of <50 bars. The densities of these fluids vary from 0.9 g/cm^3 to 1 g/cm^3 (Fig. 15b).

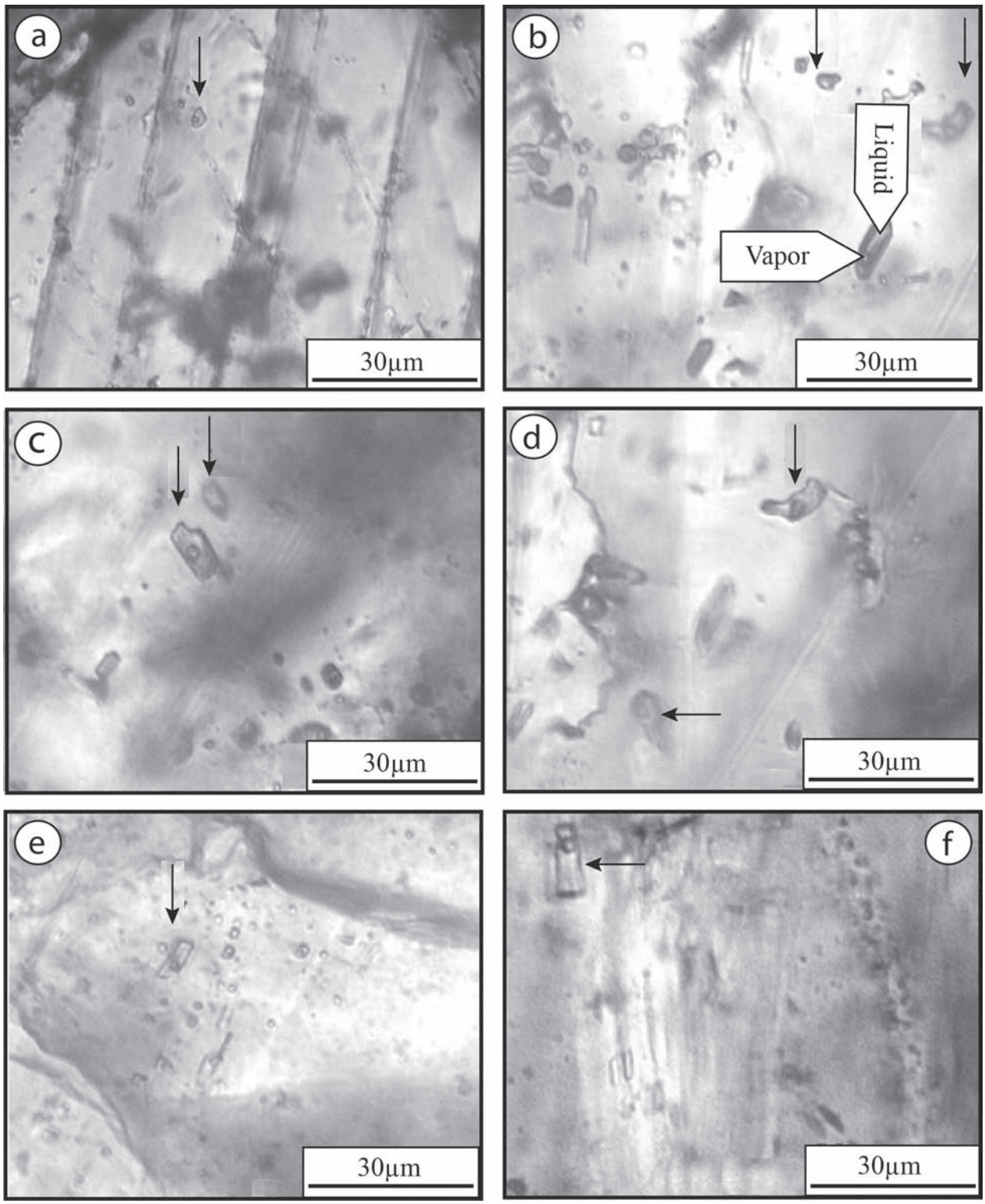

Fig. 13. Photomicrographs showing the various shapes of fluid inclusions within calcite crystals of the Mn ores at Basiran. (a, b, c, d) Elongate and stretched ellipsoidal shapes. (b) Rectangular and rod shapes. (e, c) Rhombic shape. (e, f) Trails of secondary and pseudo-secondary inclusions along microfracture surfaces.

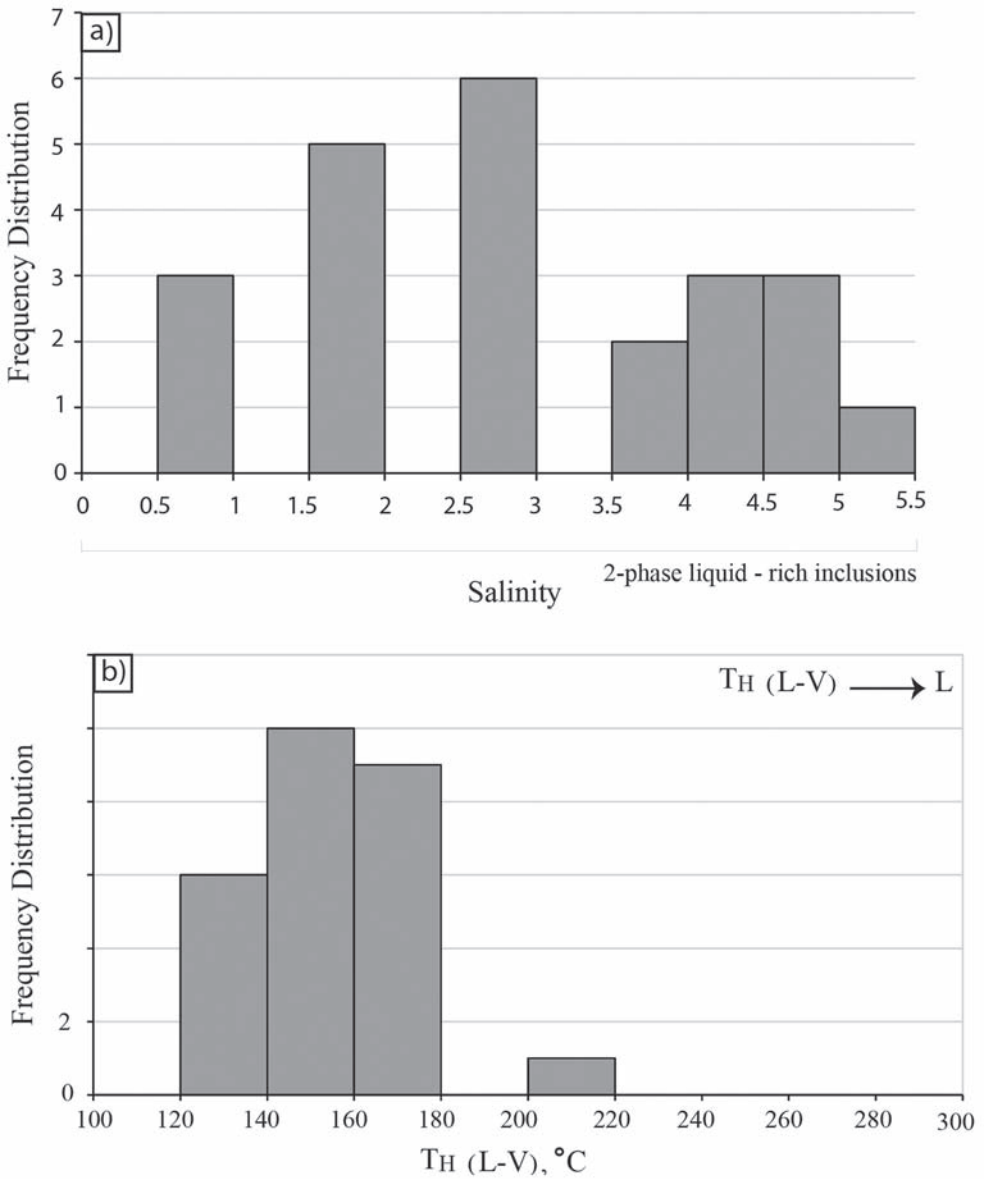

Fig. 14. (a) Frequency distribution histogram of salinities measured on liquid-rich 2-phase inclusions in calcite crystals at Basiran. (b) Frequency distribution histograms of homogenization temperatures (T_H) measured on liquid-rich 2-phase inclusions in calcite crystals at Basiran.

Genesis of the manganese ores

Based upon unequivocal geological, geochemical, and microthermometry evidence, the Mn-bearing veins formed epigenetically by hydrothermal processes. Since the dominant host rocks at Beshgaz, Sehchangi, and Basiran are andesites, it is likely that these were the potential sources of the manganese. Mn was likely leached from ferromagnesian minerals by hydrothermal fluids passing through faulted and fractured zones in the host rocks. The Mn-bearing minerals must initially have precipitated as cryptocrystalline oxyhydroxide minerals such as cryptomelane, and subsequently gradually recrystallized into psilomelane and pyrolusite over time.

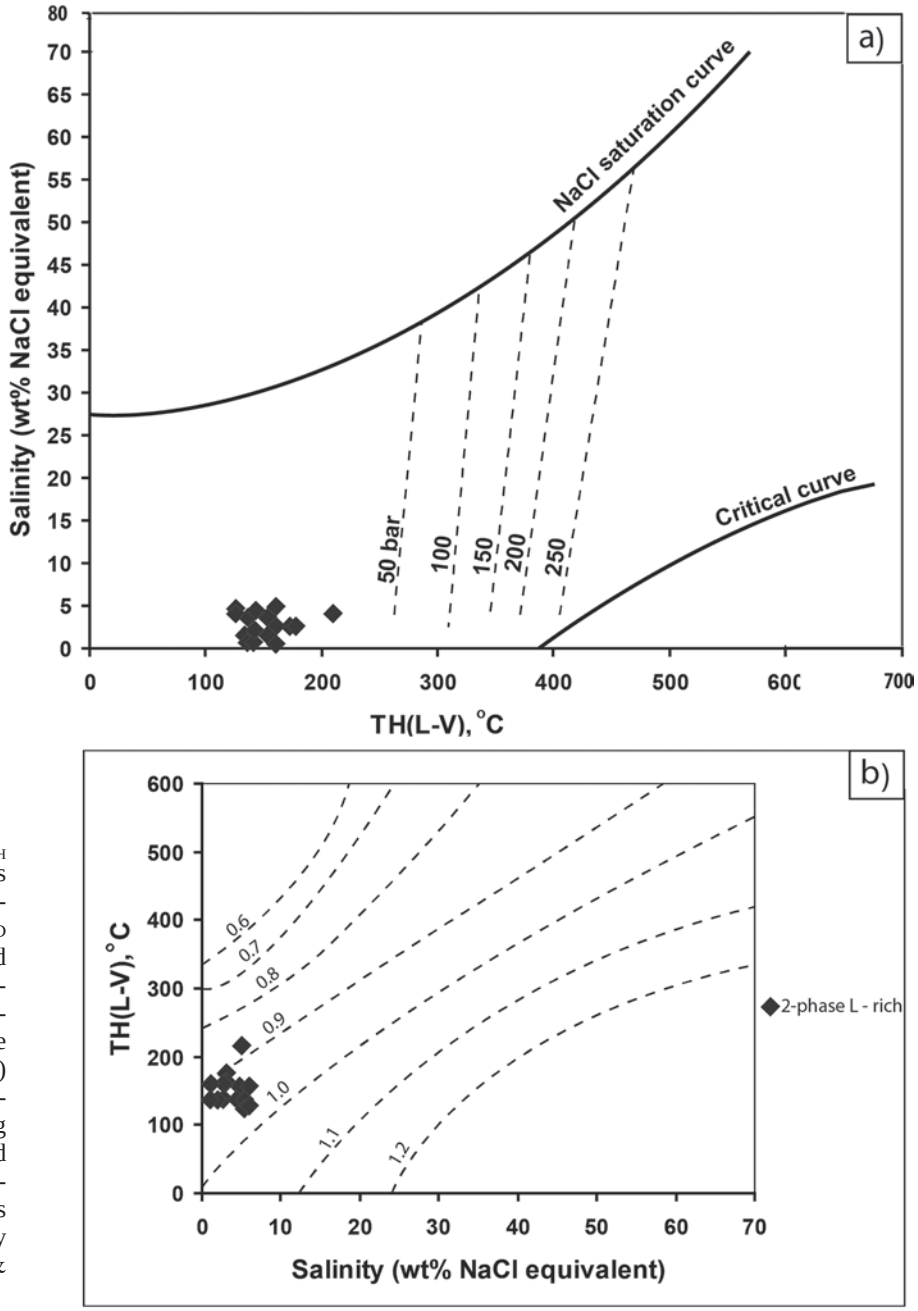

Fig. 15. (a) Bivariate plot of $T_{H\,(L–V)}$ versus salinity. Shown on this figure are also the halite saturation curve, critical curve (Ahmad & Rose 1980), and the dashed lines representing the homogenization pressures of the fluid inclusions at the indicated temperature and salinity (Roedder 1984). (b) Plot of $TH_{(L–V)}$ versus salinity (expressed as wt% NaCl eq.) showing densities (in g/cm^3) of the studied liquid-rich 2-phase fluid inclusions (Wilkinson 2001). Contours regressed from data generated by the equation-of-state of Zhang & Frantz (1987).

Conclusions

Based upon field relations, petrographic examinations, geochemical investigations, and microthermometric analysis, the following results were obtained:

1. The Mn-bearing veins in Beshgaz, Sehchangi, and Basiran prospects are hosted by volcanic and pyroclastic rocks varying in composition from rhyodacite (Eocene-Oligocene) to hornblende- and pyroxene-bearing andesite porphyries (Eocene).
2. The Mn mineralization in all three areas was recognized to be epigenetic, and having formed from hypogene hydrothermal fluids.
3. The opaque minerals are, in order of increasing abundance, pyrolusite, psilomelane and cryptomelane at Beshgaz; pyrolusite, psilomelane cryp-

tomelane, hematite, goethite and chalcopyrite at Sehchangi; and pyrolusite, psilomelane, hematite, goethite and galena at Basiran. All ores show colloidal, replacement, and open-space filling textures.

4. Major and trace element contents and ratios indicate that the Mn-bearing veins were formed by hydrothermal fluids. The average Mn grades of Mn in the Beshgaz, Sehchangi and Basiran prospects are, respectively, 25.66%, 28.10%, and 25.95%.
5. Microthermometry analyses of fluid inclusions in calcite crystals intergrown with the Mn oxides at Basiran indicate that the ore-bearing solutions had relatively low salinities (<5.5 wt% NaCl eq.) and a limited range of homogenization temperatures (TH = 120-220 °C).
6. As the rocks hosting the mineralized veins in the three prospects are similar, it seems probable that ferromagnesian minerals in the andesitic rocks acted as sources of the Mn. Leaching would have been enhanced by faulting resulting in permeable sheared and fractured zones that allowed infiltration of hydrothermal fluids.

Acknowledgements

The authors would like to acknowledge financial support provided by the Research Deputy Bureau of the University of Tabriz, We also express our thanks to the authorities of the Faculty of Sciences at University of Birjand for furnishing laboratory facilities and the experimental support by the Iran Mineral Processing Research Center (Karaj). Our appreciation is further expressed to journal reviewers Dr. S.A. Jones (Goldfields Ltd., Australia) and Dr. N Öksüz (Bozok University, Turkey) for making critical comments and suggestions to this manuscript. The authors would like to express their thanks and appreciations Dr. M.J. Timmerman (Potsdam University, Germany) for the original manuscript was improved by thoughtful and insightful and also their valuable reviews and helpful recommendations which greatly promoted the manuscript.

References

Adachi, M., Yamamoto, K. & Sugisaki, R. (1986): Hydrothermal chert and associated siliceous rocks from the northern Pacific: Their geological significance as indication of ocean ridge activity. – Sedimentary Geology, **47**: 125-148.

Ahmad, S.N. & Rose, A.W. (1980): Fluid inclusions in porphyry and skarn ore at Santa Rita, New Mexico. – Economic Geology, **75**: 229-250.

Amidi, S.M., Emami, M.H. & Michel R. (1984): Alkaline character of Eocene volcanism in the middle part of Central Iran and its geodynamic situation. – Geologische Rundschau, **73**: 917-932.

Arjmandzadeh, R., Karimpour, M.H., Mazaheri, S.A., Santos, S.A.J.F., Medina J.M. & Homam, S.M. (2011): Sr-Nd isotope geochemistry and petrogenesis of the Chah-Shaljami granitoids (Lut Block, Eastern Iran). – Journal of Asian Earth Sciences, **41**: 283-296.

Arjmandzadeh, R. & Santos, J.F. (2014): Sr–Nd isotope geochemistry and tectono-magmatic setting of the Dehsalm Cu–Mo porphyry mineralizing intrusives from Lut Block, eastern Iran. – International Journal of Earth Sciences, **103**: 123-140.

Berberian, M., Jackson, J.A., Qorashi, M., Khatib, M.M., Priestley, K., Talebien, M. & Ghafuri-Ashtiani, M. (1999): The 1997, May 10, Zirkuh (Qaenat) earthquake (M_W 7.2): Faulting along the Sistan suture zone of eastern Iran. – Geophysical Journal International, **136**: 671-694.

Camp, V.E. & Griffis, R.J. (1982): Character, genesis and tectonic setting of igneous rocks in the Sistan suture zone, eastern Iran. – Lithos, **15**: 221-239.

Choi, J.H. & Hariya, Y. (1992): Geochemistry and depositional environment of Mn oxide deposits in the Tokoro belt, northeastern Hokkaido, Japan. – Economic Geology, **87**: 1265-1274.

Crerar, D.A., Namson, J., Chyi, M.S., Williams, L. & Feigenson, M.D. (1982): Manganiferous cherts of the Franciscan assemblage: I. General geology, ancient and modern analogues, and implications for hydrothermal convection at oceanic spreading centers. – Economic Geology, **77**: 519-540.

Foerster, H. & Jafarzadeh, A. (1994): The Bafq mining district in central Iran; a highly mineralized Infracambrian volcanic field. – Economic Geology, **89**: 1697-1721.

Forster, H. (1978): Mesozoic–Cenozoic metallogenesis in Iran. – Journal of the Geological Society, **135**: 443-455.

Ghorbani, M. (2013): The Position of Iranian Mining Industry in the World. – In: Ghorbani, M. (Ed.): The Economic Geology of Iran. Springer; p. 297-332.

Hein, J.R., Koschinsky, A., Bau, M., Manheim, F.T., Kang, J.K. & Roberts, L. (2000): Cobalt rich ferromanganese crusts in the Pacific. – In: Moore, G.W. (Ed.): Handbook of Marine Mineral Deposits: 239-279; Boca Raton, Florida (CRC Press).

Holtstam, D. & Mansfeld, Y. (2001): Origin of carbonate hosted Fe-Mn-(Ba,As,Pb,Sb,W) deposit of Langbon in Central Sweden. – Mineralium Deposita, **36**: 641-657.

Jung, D., Keller, J., Khorasani, R., Marcks, Chr., Baumann, A. & Horn, P. (1983): Petrology of the Tertiary magmatic activity in the northern Lut area, East of Iran, Ministry of mines and metals. – Geological Survey of Iran, Geodynamic Project (Geotraverse) in Iran, **51**: 285-336.

Karakus, A., Yavuz, B. & Koc, S. (2010): Mineralogy and major-trace element geochemistry of the Haymana manganese mineralizations, Ankara, Turkey. – Geochemistry International, **48**: 1014-1027.

Laznicka, P. (1992): Manganese deposits in the global lithogenetic system: Quantitative approach. – Ore Geology Reviews, **7**: 279-356.

Lotfi, M. (1982): Geological and geochemical investigations on the volcanogenic Cu, Pb, Zn, Sb ore-mineralizations in the Shurab-Gale Chah and northwest of Khur (Lut,

east of Iran). – Unpublished Ph.D thesis, University of Hamburg, 151 pp.

Moore, F. & Modabberi, S. (2003): Origin of Choghart iron oxide deposit, Bafq mining district, Central Iran: new isotopic and geochemical evidence. – Journal of Sciences of Islamic Republic of Iran, **14**: 259-270.

Nicholson, K. (1992a): Contrasting mineralogical-geochemical signatures of manganese oxides: Guides to metallogenesis. – Economic Geology, **87**: 1253-1264.

Nicholson, K. (1992b): Genetic types of manganese oxide deposits in Scotland: Indicators of paleo-ocean spreading rate and a Devonian geochemical mobility boundary. – Economic Geology, **87**: 1301-1309.

Polgari, M., Hein, J.R., Vigh, T., Szabo-Drubin, M., Forizs, I., Biro, L., Muller, A. & Toth, A.L. (2012): Microbial processes and the origin of the Urkut manganese deposit, Hungary. – Ore geology, **47**: 87-109.

Richards, J.P., Spell, T., Rameh, E., Razique, A. & Fletcher, T. (2012): High Sr/Y magmas reflect arc maturity, high magmatic water content, and porphyry Cu±Mo±Au potential: examples from the Tethyan arcs of central and eastern Iran and western Pakistan. – Economic Geology, **10**: 295-332.

Roedder, E. (1976): Fluid inclusion evidence on the genesis of ores in sedimentary and volcanic rocks. – In: Wolff, K.H. (Ed.): Handbook of strata-bound and stratiform ore deposits, **2**: 67-110.

Roedder, E. (1979): Origin and significance of magmatic inclusions. – Bulletin of Mineralogy, **102**: 487-510.

Roedder, E. (1984): The Fluids in salt. – American Mineralogist, **69**: 413-439.

Rona, P.A. (1987): Criteria for recognition of hydrothermal mineral deposits in oceanic crust. – Economic Geology, **73** (2): 135-160.

Roy, S. (1992): Environments and processes of manganese deposition. – Economic Geology, **87**: 1218-1236.

Roy, S. (2012): Ancient manganese deposits. – Handbook of stratabound and stratiform ore deposits, **7**: 395-476.

Saadat, S., Stern, C.R. & Karimpour, M.H. (2008): Geochemistry of Quaternary olivine basalts from the Lut Block, eastern Iran. – American Geophysical Union, Fall Meeting 2008, abstract T21A-1933.

Saadat, S., Stern, C.R. & Karimpour, M.H. (2009): Quaternary mafic volcanic rocks along the Nayband fault, Lut block, eastern Iran. – Geological Society of America Annual Meeting: 18-21.

Samani, B.A. (1988): Metallogeny of the Precambrian in Iran. – Precambrian Research **39**: 85-106.

Shah, M.T. & Khan, A. (1999): Geochemistry and origin of Mn-deposits in the Waziristan ophiolite complex, North Waziristan, Pakistan. – Mineralium Deposita, **34**: 697-704.

Spooner, E.T.C. (1981): Fluid inclusion studies of hydrothermal ore deposits. In: Short Course in fluid Inclusions. – In: Hollister. L.S. & Crawford, M.L. (Eds.): Fluid inclusions: applications to petrology. Mineralogical Association of Canada Short Course Handbook, **6**: 209-240.

Tarkian, M., Lotfi, M. & Baumann, A. (1983): Tectonic, magmatism and the formation of mineral deposits in the central Lut, east Iran, Ministry of mines and metals. Geological survey of Iran, Geodynamic Project (Geotraverse) (in Persian), **51**: 357-383.

Tirrul, R., Bell, I.R., Griffis, J.R. & Camp V.E. (1983): The Sistan suture zone of Eastern Iran. – Geological Society of America Bulletin, **94**: 134-150.

Toth, J.R. (1980): Deposition of submarine crusts rich in manganese and iron. – Geological Society of America Bulletin, **91**: 44-54.

Walker, R.T., Gans, P., Allen, M.B., Jackson, J., Khatib, M., Marsh, N. & Zarrinkoub, M. (2009): Late Cenozoic volcanism and rates of active faulting in eastern Iran. – Geophysical Journal International, **177**: 783-805.

Wilkinson, J.J. (2001): Fluid inclusions in hydrothermal ore deposits. – Lithos, **55**: 229-272.

Zhang, Y.G. & Frantz, J.D. (1987): Determination of the homogenization temperatures and densities of supercritical fluids in the system NaCl–KCl–$CaCl_2$–H_2O using synthetic fluid inclusions. – Chemical Geology, **64**: 335-350.

Manuscript received: July, 5th, 2017.
Revised version accepted by the Potsdam editor: August 23th, 2017.

Addresses of the authors:

Behnaz Barghi (corresponding author), Ali Asghar Calagari, Department of Earth Sciences, Faculty of Natural Sciences, University of Tabriz, Tabriz 51666-16471, Iran.
E-mail: barghibehnaz@yahoo.com

Mohammad Hossein Zarrinkoub, Geology Department, University of Birjand, Iran.

Vartan Simmonds, Research Institute for Fundamental Sciences, University of Tabriz, Tabriz 51668-76393, Iran.

Table 1. Chemical analyses of major, minor and trace elements in the Mn ores from the studied areas (Beshgaz, Sehchangi, and Basiran) obtained by the ICP-ES-MS and ICP-MS methods. MDL = minimum detection limit.

		Beshgaz							Jonub-e sehchangi							Basiran		
	*MDL ppm	B-06.1	B-06.2	B-09	B-02	B-01	B-03	B-08	J-97	J-100.1	J-100.2	J-100.3	J-105	J-98	J-96	Ba-18	Ba-20	Ba-30
Mo	0.5	790.3	147.2	202.9	148.3	77.3	135.4	101.8	26.2	15.9	15.4	22.3	18.8	23.6	12.0	9.5	3.9	4.7
Cu	0.5	20.8	18.6	23.8	18.4	18.9	22.8	43.3	353.0	289.7	287.8	276.7	288.9	858.7	1999.9	33.5	17.6	47.6
Pb	0.5	6.6	29.5	41.5	24.2	145.5	10.5	23.5	190.9	127.6	144.6	110.2	126.8	244.0	856.6	23955.6	6417.4	>100000
Zn	5	526	504	439	336	523	188	101	614	353	347	433	505	869	1489	17948	48994	52808
Ag	0.5	<0.5	<0.5	<0.5	<0.5	0.5	<0.5	<0.5	<0.5	<0.5	<0.5	<0.5	<0.5	<0.5	<0.5	72.2	1.9	>300
Ni	0.5	75.2	158.3	59.3	51.2	79.7	36.8	38.3	44.4	28.0	31.8	38.2	38.4	42.7	39.1	52.3	54.5	9.4
Co	1	1852	1509	844	1204	1320	396	297	24	13	15	15	16	43	61	11	13	10
As	5	41	16	33	29	33	11	68	13871	11286	8937	7642	14269	32371	45133	77	10	14
U	0.5	4.3	3.9	2.8	5.2	4.3	0.6	1.1	7.4	3.5	3.3	3.3	5.9	3.1	3.7	4.0	2.9	2.1
Th	0.5	4.0	12.3	11.2	10.6	10.8	1.4	0.7	0.6	0.5	0.8	1.1	2.1	4.4	4.9	<0.5	<0.5	<0.5
Sr	5	1694	1696	1061	1623	1880	409	333	2430	2284	1999	744	1681	1670	1990	1328	1356	1194
Cd	0.5	5.3	3.5	3.0	4.9	6.7	1.2	1.1	<0.5	<0.5	<0.5	<0.5	<0.5	<0.5	<0.5	35.6	83.8	91.0
Sb	0.5	5.3	1.9	5.5	4.9	3.7	4.0	9.2	788.8	694.2	675.0	599.9	719.2	327.6	262.2	6.4	2.8	396.5
Bi	0.5	<0.5	<0.5	<0.5	<0.5	<0.5	<0.5	<0.5	<0.5	<0.5	<0.5	<0.5	<0.5	<0.5	<0.5	<0.5	2.1	<0.5
V	10	554	49	160	118	71	203	317	226	100	99	97	147	271	183	<10	14	<10
La	0.5	14.2	36.4	39.9	22.7	34.1	4.5	9.6	4.6	4.9	5.9	5.7	7.2	10.5	12.9	5.6	18.7	4.3
Cr	1	12	10	15	26	13	33	130	17	19	20	24	20	36	27	54	16	192
Ba	5	13859	4789	3711	2171	960	786	1479	20040	6853	7652	7915	12797	8503	8650	25	47	26
W	0.5	1.7	4.0	2.9	1.5	1.6	1.0	12.1	324.5	178.5	210.9	179.8	208.6	155.5	59.9	<0.5	0.9	<0.5
Zr	0.5	215.3	132.4	174.4	149.0	111.6	136.2	75.5	6.9	6.5	7.7	11.3	16.1	40.4	37.3	0.8	7.5	7.2
Ce	5	21	81	91	41	53	17	13	6	<5	6	8	11	19	23	13	34	10
Sn	0.5	1.1	2.3	2.0	2.4	2.2	0.6	2.0	<0.5	<0.5	<0.5	<0.5	<0.5	0.7	0.6	1.3	2.2	28.0
Y	0.5	46.0	63.9	43.8	41.3	60.1	10.9	97.8	6.1	6.6	5.8	6.8	8.3	11.5	12.7	13.8	21.6	17.3
Nb	0.5	9.9	10.9	11.8	11.3	8.0	4.0	4.6	<0.5	<0.5	0.6	0.9	1.5	3.5	2.9	<0.5	2.1	1.8
Ta	0.5	<0.5	0.8	0.7	0.7	0.7	<0.5	<0.5	<0.5	<0.5	<0.5	<0.5	<0.5	<0.5	<0.5	<0.5	<0.5	<0.5
Be	5	15	5	12	13	13	<5	<5	10	11	11	10	9	<5	6	<5	<5	<5
Sc	1	6	4	6	6	6	3	1	2	2	3	5	3	9	12	2	9	2
Li	0.5	5.3	14.9	8.2	8.7	11.2	2.1	3.6	16.1	14.6	26.2	26.5	22.2	67.3	31.0	27.0	86.6	81.1
Rb	0.5	44.8	80.7	77.6	97.1	76.7	24.0	17.8	35.6	24.1	33.4	22.3	107.4	109.6	110.2	5.7	4.8	3.9
Hf	0.5	1.1	2.9	2.4	2.4	2.0	0.7	<0.5	<0.5	<0.5	<0.5	<0.5	0.6	1.3	1.0	<0.5	<0.5	<0.5
Se	5%	<5	<5	<5	<5	<5	<5	<5	<5	<5	<5	<5	<5	<5	<5	<5	<5	<5
Ti	0.01	0.029	0.074	0.072	0.093	0.050	0.027	0.010	0.031	0.031	0.041	0.048	0.094	0.219	0.192	0.017	0.043	0.039
Al	0.01	1.44	4.26	3.98	4.32	3.78	0.75	0.40	0.75	0.69	0.86	1.08	1.96	4.34	4.52	0.17	0.43	0.47
Na	0.01	0.63	1.55	1.36	1.63	1.30	0.19	0.07	0.33	0.23	0.31	0.30	0.20	0.47	0.80	0.67	0.28	0.06
K	0.01	3.32	3.29	3.28	3.20	3.11	1.21	1.06	0.89	0.53	0.72	0.47	2.40	2.98	2.54	0.15	0.13	0.07
Ca	0.01	0.49	0.73	0.64	0.91	0.55	0.25	0.17	4.87	6.13	5.46	9.77	8.52	4.23	10.46	2.78	0.47	2.60
P	0.01	0.33	0.09	0.20	0.16	0.20	0.08	0.09	0.02	0.02	0.02	0.02	0.03	0.05	0.04	<0.01	0.02	0.01
Mg	0.01	0.22	0.32	0.35	0.14	0.39	0.16	0.04	0.47	0.36	0.44	0.56	0.49	0.26	0.67	0.51	0.27	0.10
Mn	0.01	45.25	26.28	27.50	21.77	32.58	11.66	10.60	40.82	36.40	35.85	33.02	28.56	15.78	6.293	28.49	29.71	19.67
Fe	0.01	0.64	1.16	0.84	1.77	1.00	1.11	3.82	0.36	0.41	0.53	0.86	1.24	2.56	2.54	22.26	21.08	7.15
SiO2	0.01	5.29	21.32	16.92	27.31	17.53	43.83	44.92	4.87	8.03	7.22	7.32	9.97	21.22	18.04	3.15	7.83	4.78
Si/Al		1.71	2.33	1.98	2.95	2.16	27.30	52.46	3.02	5.43	3.91	3.15	2.37	2.28	1.86	8.65	8.50	4.75
Mn/Fe		70.70	22.65	31.73	12.29	32.58	10.50	2.77	113.38	88.78	67.64	38.39	23.03	6.16	2.47	1.28	1.40	2.75

Table 2. Microthermometry data obtained from fluid inclusions within calcite crystals in the Mn ores at Basiran.

n	Size (μm)	Type	Te (°C)	Tmice (°C)	wt% NaCl	Thv-l (°C)
1	5	L+V		.....	.....	130
2	5	L+V		.....	.....	140
3	6	L+V		.....	.....	140
4	10	L+V		-2.5	4.24	207
5	7	L+V		-2.7	4.58	130
6	5	L+V		-3	5.07	130
7	7	L+V		-2.7	4.58	160
8	10	L+V		-2.6	4.41	144
9	9	L+V		-2.5	4.24	140
10	7	L+V		-2.7	4.58	130
11	7	L+V		-1.5	2.5	140
12	7	L+V		-2.3	3.9	158
13	6	L+V		-1.2	1.94	150
14	7	L+V		-0.5	0.6	139
15	5	L+V	-21	-0.5	0.6	145
16	10	L+V		-2.1	3.56	142
17	5	L+V		-1	1.57	135
18	7	L+V		-0.5	0.6	160
19	8	L+V		-1.5	2.5	163
20	10	L+V		-1.2	1.94	160
21	10	L+V		-1.2	1.94	160
22	10	L+V		-1	1.57	160
23	10	L+V		-1.5	2.5	165
24	8	L+V		-1.5	2.5	178
25	5	L+V		-1.2	2.5	145
26	5	L+V		-1.5	2.5	175